THE JOURNAL OF BIOLOGICAL CHEMISTRY VOL. 288, NO. 9, pp. 6083–6094, March 1, 2013

HIV-1 Viral Infectivity Factor (Vif) Alters Processive Single-stranded DNA Scanning of the Retroviral Restriction Factor APOBEC3G*[S]

Received for publication, September 21, 2012, and in revised form, January 11, 2013 Published, JBC Papers in Press, January 11, 2013, DOI 10.1074/jbc.M112.421875

Yuqing Feng, Robin P. Love, and Linda Chelico[1]

From the Department of Microbiology and Immunology, University of Saskatchewan, Saskatoon, Saskatchewan S7N 5E5, Canada

Background: Retroviral restriction factor APOBEC3G is inhibited from inducing mutations in HIV-1 proviral DNA in multiple ways by HIV-1 Vif.
Results: Vif-mediated inhibition of APOBEC3G deoxycytidine deaminase activity is due to a change in APOBEC3G processive scanning.
Conclusion: Altered processivity leads to a decrease in deoxycytidine deamination-induced mutagenesis.
Significance: Vif co-encapsidation with APOBEC3G in virions may promote sublethal mutagenesis of proviral DNA.

APOBEC3G is a retroviral restriction factor that can inhibit the replication of human immunodeficiency virus, type 1 (HIV-1) in the absence of the viral infectivity factor (Vif) protein. Virion-encapsidated APOBEC3G can deaminate cytosine to uracil in viral (−)DNA, which leads to hypermutation and inactivation of the provirus. APOBEC3G catalyzes these deaminations processively on single-stranded DNA using sliding and jumping movements. Vif is thought to primarily overcome APOBEC3G through an interaction that mediates APOBEC3G ubiquitination and results in its proteasomal degradation. However, Vif may also inhibit APOBEC3G mRNA translation, virion encapsidation, and deamination activity. Here we investigated the molecular mechanism of Vif_{IIIB}- and Vif_{HXB2}-mediated inhibition of APOBEC3G deamination activity. Biochemical assays using a model HIV-1 replication assay and synthetic single-stranded or partially double-stranded DNA substrates demonstrated that APOBEC3G has an altered processive mechanism in the presence of Vif. Specifically, Vif_{HXB2} inhibited the jumping and Vif_{IIIB} inhibited the sliding movements of APOBEC3G. The absence of such an effect by Vif on degradation-resistant APOBEC3G D128K indicates that a Vif-APOBEC3G interaction mediates this effect. That the partially processive APOBEC3G was less effective at inducing mutagenesis in a model HIV-1 replication assay suggests that Vif co-encapsidation with APOBEC3G can promote sublethal mutagenesis of HIV-1 proviral DNA.

APOBEC3G (A3G)[2] is a single-stranded DNA (ssDNA) deoxycytidine deaminase that functions as a potent host restriction factor to inhibit HIV-1 replication in strains that lack the viral infectivity factor (Vif) (1–4). In the absence of Vif, sufficient amounts of A3G are able to become incorporated into budding virions by binding to the viral genomic (+)RNA or 7SL cellular RNA and/or nucleocapsid portion of the Gag (5). Subsequently, A3G catalyzes the deamination of cytosine to uracil (C→U) on nascently formed viral (−)DNA in the target cell (6, 7). HIV-1 reverse transcriptase (RT) uses these uracils as a template, thereby creating G→A mutations on the viral genomic strand, resulting in hypermutation and inactivation of proviral DNA (2–4). Synthesis of the (−)DNA is initiated from a host $tRNA_3^{Lys}$ primer that binds the HIV-1 primer binding site near the 5′-end of the viral genome (8). Two polypurine tracts (PPTs) that reside in the center and the 3′-end of the HIV-1 RNA genome are responsible for priming (+)DNA synthesis by virtue of their resistance to RNase H degradation (9). The multiple priming sites for (+)DNA synthesis allow for conversion of the single-stranded (−)DNA to a double-stranded DNA (dsDNA) provirus as rapidly as possible and influence the distribution of A3G-induced mutations (10, 11).

A3G is able to search for its preferred 5′-CC<u>C</u> or 5′-C<u>C</u> deamination motif (the underlined C is deaminated) using a processive scanning mechanism (12). The scanning appears to be through facilitated diffusion (13–15) and involves sliding and microscopic jumping movements (12, 16, 17) that enable a three-dimensional search of the ssDNA without A3G diffusing into the bulk solution. This searching mechanism gives enzymes the potential to increase their target searching efficiency (13, 15) and results in A3G-catalyzed deaminations occurring in a stochastic manner (18). Furthermore, because A3G must scan viral (−)DNA in the presence of short RNA/DNA hybrid regions that result from incomplete processing by the RT RNase H domain, the three-dimensional search enables an efficient scan of the heterogenous substrate (19). A3G contains two zinc binding domains. The C-terminal half contains the catalytically active (catalytic domain 2) domain that is

* This work was supported by Canadian Institutes of Health Operating Grant HOP-111407, a new investigator establishment grant from the Saskatchewan Health Research Foundation, the Canadian Foundation for Innovation, and the Tri-Link Biotechnologies Research Rewards Program.
⌘ *Author's Choice*—Final version full access.
[S] This article contains supplemental Experimental Procedures, Figs. S1–S3, and Tables S1–S4.
[1] To whom correspondence should be addressed. Tel.: 306-966-4318; Fax: 306-966-4298; E-mail: linda.chelico@usask.ca.
[2] The abbreviations used are: A3G, APOBEC3G; ss, single-stranded; Vif, viral infectivity factor; RT, reverse transcriptase; *prot*, protease; F, fluorescein; K_d, apparent dissociation constant; HIV-1, human immunodeficiency virus, type 1; PPT, polypurine tract; nt, nucleotide(s).

directly responsible for deaminase activity of A3G (20, 21) and can contribute to oligomerization (22–25). The N-terminal half (catalytic domain 1) is catalytically inactive, but this half of the enzyme is responsible for processivity and virion encapsidation and can also mediate oligomerization of A3G (19–21, 25–27). The residues that appear to contribute to these functions of the N-terminal half are located on predicted loop 7, residues 124–130 (19, 26, 27) (supplemental Fig. S1).

A3G-mediated restriction of HIV-1 is for the most part inhibited by HIV-1 Vif (28–32). Vif is thought to primarily accomplish this through triggering A3G degradation (29–32). Among the seven APOBEC3 family members (A3A, A3B, A3C, A3D, A3F, A3G, and A3H), A3G appears to be the most potent at restricting HIV-1 (33–35) but also the most sensitive to Vif (36). Specifically, Vif binds to A3G (30–32), is stabilized in host cells by binding the transcription cofactor core-binding factor-β (37, 38), and recruits a cellular ubiquitin ligase complex (29). This results in the polyubiquitination and degradation of A3G through the 26 S proteasome pathway (39, 40). Vif inhibits the antiviral activity of A3G in a species-specific manner (41). For example, HIV-1 Vif fails to neutralize A3G from African green monkey or rhesus macaque, and conversely, simian immunodeficiency virus Vif is incapable of neutralizing human A3G (41). This species-specific type of A3G restriction has been correlated with the ability of Vif to physically associate with A3G and is centrally mediated by Asp^{128} of A3G (42). Mutating human A3G Asp^{128} to Lys as is found in African green monkey A3G abrogates the effect of HIV-1 Vif on human A3G (42–44). The Asp^{128} is predicted to be located on loop 7 in the N-terminal half of A3G (supplemental Fig. S1) near the determinants for dimerization, processivity, and virion incorporation (^{124}YYFW^{127}) (19, 26, 27).

Additionally, Vif has been shown to inhibit A3G function in two other ways that appear to involve the RNA binding ability of Vif. First, Vif has been reported to promote A3G virion exclusion in a degradation-independent manner (28, 45–48). A3G needs to bind to the viral genomic RNA or cellular 7SL RNA and/or the nucleocapsid portion of HIV-1 Gag to be encapsidated in the budding virus (5). It has been suggested that Vif recruits A3G into high molecular weight RNA/protein masses that are unable to be encapsidated, but the exact mechanism has not been identified (49). Vif may exert this function as a secondary effect of its own attempt to be encapsidated into budding virions, although the amount of Vif estimated in virions ranges widely from about seven to 80 molecules (50–53). Second, there is evidence to suggest that Vif depletes the intracellular pool of A3G by down-regulating its mRNA translation and stability (30, 46, 54). It is thought that Vif can directly bind A3G mRNA to exert this function (54).

Despite the multiple ways Vif attempts to inhibit A3G virion encapsidation, Vif neutralization of A3G may not be absolute. A3G may be capable of escaping Vif inhibition in the virus-producing cell, resulting in A3G encapsidation into budding virions (55, 56). Nowarski *et al.* (56) reported that a range of 0.3–0.8 molecules of A3G can be found in wild type (WT) HIV-1 virions, far less than the four to nine molecules of A3G found in Vif-deficient virions (57). Furthermore, the residual A3G encapsidated with Vif in the virion was found to be less catalytically active than A3G encapsidated in its absence (58). The explanation of this observation is that virus-encapsidated Vif inhibits A3G deamination activity (58). This is supported by an earlier report that characterized this phenomenon when A3G and Vif were co-expressed in *Escherichia coli* (59). The mechanism by which Vif inhibits A3G deamination activity is not fully understood. However, this mode of Vif-mediated inhibition has implications for the design of Vif-based HIV-1 therapeutics that exclude Vif from interacting with ubiquitin ligase components but allow it to remain in contact with A3G (60, 61) and the relationship between A3G deamination activity and sublethal mutagenesis of HIV-1 (55, 62–64). Vif-mediated partial inhibition of A3G deamination activity could lead to viral evolution rather than viral inactivation.

Here we investigate the molecular mechanism of degradation-independent Vif-mediated inhibition of A3G deamination activity. Two Vif variants, Vif_{HXB2} and Vif_{IIIB}, were applied in our study. We used Vif_{IIIB} as a standard variant from a widely used HIV-1 laboratory isolate (NL4-3), and we used Vif_{HXB2} because it has been reported to be more potent at Vif-mediated degradation of APOBEC3 enzymes (36). The data indicate that the Vif variants inhibited A3G deamination activity by primarily altering its processive scanning mechanism, which decreased the ability of A3G to induce mutations in nascently reverse transcribed cDNA. Each Vif variant could inhibit A3G processive scanning in a unique way, suggesting that there are variant-specific interactions that underlie the differential potency of Vif_{HXB2} and Vif_{IIIB} against APOBEC3 enzymes (36).

EXPERIMENTAL PROCEDURES

Protein Expression and Purification—Recombinant baculovirus production for expression of GST-A3G, GST-A3G D128K, GST-Vif_{IIIB}, GST-Vif_{HXB2}, or GST-nucleocapsid protein in *Sf*9 cells was carried out using the transfer vector pAcG2T (BD Biosciences) as described previously (12, 19). Vif_{IIIB} was cloned from the pcDNA-hVif vector encoding the Vif protein of HIV-1 NL4-3 that was obtained from the AIDS Research and Reference Reagent Program, Division of AIDS, NIAID, National Institutes of Health from Dr. Stephan Bour and Dr. Klaus Strebel (65). Vif_{HXB2} was cloned from pHIV-*gpt*(WT), a gift from Dr. David Kabat (Oregon Health and Science University). Site-directed mutagenesis was used to create the A3G D128K clone. Cloning primers for Vif variants and the site-directed mutagenesis primers were obtained from Integrated DNA Technologies and are listed in supplemental Table S1. *Sf*9 cells were infected with recombinant virus at a multiplicity of infection of 1, except for GST-Vif_{IIIB} and GST-Vif_{HXB2}, which were infected at a multiplicity of infection of 4 or 2, respectively. Recombinant baculovirus-infected *Sf*9 cells were harvested after 72 h of infection, except for GST-Vif_{IIIB} and GST-Vif_{HXB2}, which were harvested after 48 h of infection. Cells were lysed in the presence of RNase A, and the proteins (A3G, A3G D128K, and nucleocapsid protein) were purified as described previously (22) to obtain protein that was cleaved from the GST tag and 95% pure. The Vif variants were eluted from the glutathione-Sepharose resin (GE Healthcare) as described previously (12) with the GST tag to maintain their stability. Eluted GST-Vif variants were dialyzed against 100 mM

Tris, pH 7.5, 250 mM NaCl, 10% glycerol, and 1 mM DTT and were 85% pure. Protein fractions were stored at −80 °C. HIV-1 reverse transcriptase p66/p51 (66) was generously provided by Dr. Stuart F. J. Le Grice (NCI, National Institutes of Health).

Model HIV-1 Replication Assay—The model HIV-1 replication assay, which measures A3G-induced mutagenesis of ssDNA during reverse transcription of an RNA template, was performed as described previously (19). A synthetic (+)RNA genome that contains a PPT, 120 nt of the catalytic domain of the HIV-1 protease (*prot*), and *lacZα* (248 nt) was synthesized *in vitro*. The PPT enabled second strand ((+)DNA) synthesis to occur. The *lacZα* was used as a reporter gene for mutations by blue/white screening. The originating sequence of the HIV-1 protease gene is from a clone obtained through the AIDS Research and Reference Reagent Program, Division of AIDS, NIAID, National Institutes of Health, p93TH253.3 from Dr. Feng Gao and Dr. Beatrice Hahn (67). The RNA template (25 nM) was annealed to a 24-nt DNA primer (19) and incubated with nucleocapsid protein (1.5 μM), RT (1.2 μM), and dNTPs (500 μM) in RT buffer (50 mM Tris, pH 7.4, 40 mM KCl, 10 mM $MgCl_2$, and 1 mM DTT) in the presence or absence of 100 nM A3G or A3G D128K. A3G, RT, and nucleocapsid protein were added to the reaction at ratios to the RNA that are estimated to be found in virions (8, 57, 68, 69). Reactions containing A3G or A3G D128K were conducted in the presence or absence of 175 nM Vif_{IIIB} or Vif_{HXB2}. Synthesized DNA was PCR-amplified using *Pfu* Turbo C_x (Agilent Technologies) and cloned into a pETBlue-1 vector backbone that allows the experimentally synthesized *lacZα* to be used for α-complementation (19). Twenty-five mutated clones for each condition tested were analyzed. DNA sequencing was carried out at the National Research Council of Canada (Saskatoon, Saskatchewan). A *t* test was used for statistical analysis of sequences.

Deamination Assays—The 118-nt ssDNA substrate was obtained from Tri-Link Biotechnologies, and the sequence is listed in supplemental Table S1. A3G and A3G D128K (10-20 nM) were incubated with 100 nM fluorescein (F)-labeled ssDNA and 700 nM Vif (IIIB or HXB2) in RT buffer. The substrate to A3G ratio was kept high to ensure that reactions were carried out under single hit conditions, *i.e.* <15% substrate consumed (70), where a single A3G could interact with a particular ssDNA substrate once at most. Reactions were incubated at 37 °C for 2.5–40 min. Deaminations were detected by resolving DNA that had been treated with uracil-DNA glycosylase and heated under alkaline conditions on a 10% (v/v) denaturing polyacrylamide gel as described previously (12). Gel pictures were obtained using a Typhoon Trio (GE Healthcare) multipurpose scanner, and analysis of integrated gel band intensities was performed using ImageQuant software (GE Healthcare). Under these conditions, a processivity factor can be determined by comparing the total number of deaminations occurring at two sites on the same DNA substrate with a calculated theoretical value of the expected deaminations that would occur at those two sites if the events were uncorrelated, *i.e.* not processive (see Ref.12). The specific activity was calculated from single hit condition reactions by determining the picomoles of substrate consumed/minute for a microgram of enzyme. The addition of DNA was used to start the deamination reactions. Prior to the addition of DNA, the reaction components were prewarmed to 37 °C.

Steady State Rotational Anisotropy Assays—Steady state fluorescence depolarization (rotational anisotropy) was used to measure protein-nucleic acid and protein-protein binding affinities using an F-labeled binding partner. A QuantaMaster QM-4 spectrofluorometer (Photon Technology International) with a dual emission channel was used to collect data and calculate anisotropy. Measurements were made at 21 °C. Samples were excited with vertically polarized light at 495 nm (6-nm band pass) and vertical and horizontal emissions were measured at 520 nm (6-nm band pass). Apparent dissociation constants (K_d) were obtained by fitting to a rectangular hyperbola or sigmoidal curve using SigmaPlot 11.2 software.

A3G, A3G D128K, Vif_{IIIB}, and Vif_{HXB2} were tested for their ability to bind the ssDNA substrates 118-nt ssDNA and *prot* (−)DNA, which are listed in supplemental Table S1 and described in the text. Reactions were 50 μl and contained F-labeled ssDNA (50 nM) in RT buffer, and A3G (0–700 nM) or Vif (0–200 nM) was titrated into the reaction. Alternatively, A3G or D128K was mixed with a Vif variant at an equimolar ratio before titration (0–350 nM) into the reaction.

For protein-protein binding, A3G or A3G D128K was labeled with fluorescein using the Fluorescein-EX Protein Labeling kit (Invitrogen). The F-A3G or F-D128K (50 nM) was used in a reaction mixture (50 μl) that contained RT buffer and a titration of Vif_{IIIB} or Vif_{HXB2} (0–200 nM).

RESULTS

Decreased A3G-induced Mutagenesis in the Presence of Vif—A reconstituted model HIV-1 replication system was used to determine whether Vif could inhibit the deamination ability of A3G. In this assay, we used an RNA construct that contains (from the 5′- to 3′-end) a PPT, 120 nt of the HIV-1 *prot* active site, and the *lacZα* gene. The PPT enables second strand synthesis to occur. The *prot* and *lacZα* sequences are used to characterize the spectra of mutations. The *prot* sequence is further used to gauge the ability of A3G-induced deaminations to inactivate the protease enzyme. As such, the sequence is analyzed in the (+)strand orientation where C→U deaminations are detected as G→A mutations. A3G was able to cause an approximately 17-fold increase in the population mutation frequency and an 11-fold increase in the clone mutation frequency as compared with RT alone (compare Table 2 and supplemental Table S2).

A plot of the distribution of A3G-induced mutations recovered from the sequenced clones demonstrates a mutational gradient in the 5′ → 3′ orientation, meaning that deaminations were biased toward the 5′-end of the nascently synthesized cDNA (Fig. 1*A*). This has been observed previously for A3G *in vivo* due to HIV-1 replication dynamics in which (−)DNA furthest from the PPT is single-stranded the longest and incurs the most deaminations (7, 10, 11). To determine whether Vif could influence the deamination activity of A3G, we added Vif at excess (~2-fold more than A3G). It can be seen by visual inspection of the mutation spectra that addition of Vif_{IIIB} or Vif_{HXB2} caused a decrease in A3G-induced mutagenesis (Fig. 1*A*) with Vif_{HXB2} (Fig. 1*B*) having a greater inhibitory effect

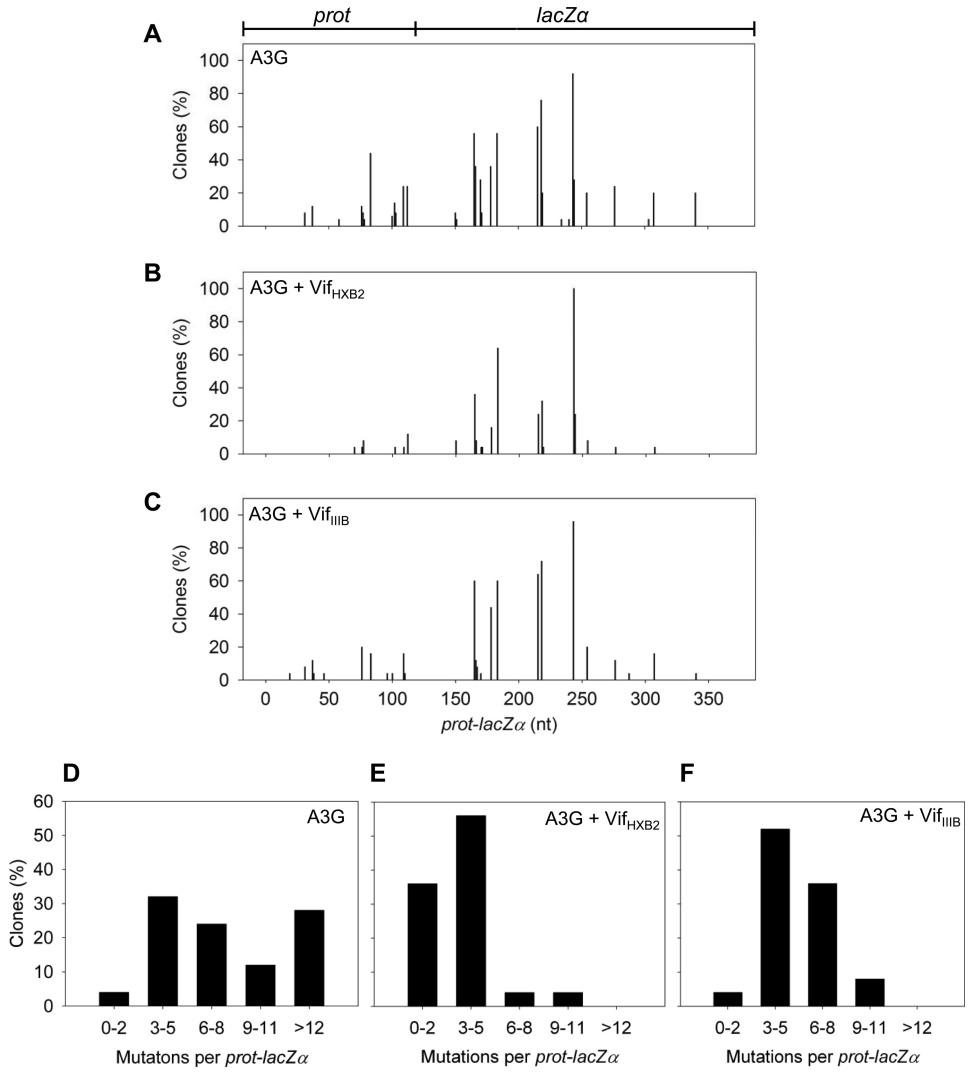

FIGURE 1. **A3G-induced mutagenesis is inhibited by Vif$_{HXB2}$ and Vif$_{IIIB}$ in a model HIV-1 replication system.** *A–C*, spectra of mutations incurred in the 368-nt *prot-lacZα* construct are plotted as the percentage of clones containing a mutation at a particular location (nt) for A3G (*A*), A3G in the presence of Vif$_{HXB2}$ (*B*), and A3G in the presence of Vif$_{IIIB}$ (*C*). *D–F*, histograms were generated to illustrate the population distribution of mutations per *prot-lacZα* construct for A3G (*D*), A3G in the presence of Vif$_{HXB2}$ (*E*), and A3G in the presence of Vif$_{IIIB}$ (*F*).

than Vif$_{IIIB}$ (Fig. 1*C*). The decrease in the A3G-induced mutations when Vif$_{HXB2}$ (Fig. 1*B*) or Vif$_{IIIB}$ (Fig. 1*C*) was present was greater in the *prot* likely because of the shorter time that this region is single-stranded in comparison with the *lacZα* due to the proximity to the PPT. The clones were also binned for analysis based on the number of mutations per *prot-lacZα* (Fig. 1, *D–F*). A3G was able to induce a widespread number of mutations. We found a range of 3–12 mutations per *prot-lacZα* occurring for A3G (Fig. 1*D*). The data are far less spread when A3G-induced mutagenesis occurred in the presence of Vif$_{HXB2}$ where we found only three to five mutations per *prot-lacZα* ~55% of the time and 0–2 mutations per *prot-lacZα* ~35% of the time (Fig. 1*E*). For Vif$_{IIIB}$, the reduction in A3G-induced mutations is demonstrated by a shift of mutations down to three to eight mutations per *prot-lacZα* (Fig. 1*F*). The data were analyzed further by comparing the frequency of mutations in heavily mutated sites in the presence of A3G and the in absence and presence of Vif (Table 1). From this analysis, we found that Vif$_{HXB2}$ caused six of the eight heavily mutated sites to be mutated at a lower level (Table 1, A3G + Vif$_{HXB2}$). The detrimental effect of Vif$_{IIIB}$ on A3G-induced mutagenesis was only significant in the *prot* region (Table 1, A3G + Vif$_{IIIB}$).

TABLE 1

Frequency of A3G hot spot mutations in the prot-lacZα

A hot spot was defined as occurring in at least 20% of clones for the *prot* region (1–120 nt) and at least 50% of clones for the *lacZα* region (121–368 nt).

Site	Frequency of mutation		
	A3G	A3G + Vif$_{HXB2}$	A3G + Vif$_{IIIB}$
nt			
85	0.44	0.00[a]	0.16[b]
111	0.24	0.04[b]	0.16[c]
114	0.24	0.12[c]	0.00[b]
166	0.56	0.36[b]	0.60
184	0.56	0.64[c]	0.60
216	0.60	0.24[b]	0.64
219	0.76	0.32[a]	0.72
244	0.92	1.00	0.96

[a] Significant difference was designed as $p \leq 0.001$ *versus* A3G values.
[b] Significant difference was designed as $p \leq 0.01$ *versus* A3G values.
[c] Significant difference was designed as $p \leq 0.05$ *versus* A3G values.

The more potent effect of Vif$_{HXB2}$ was further evident when the mutation frequencies were examined. Here we scored the

TABLE 2

A3G-mediated mutation frequencies in a model HIV-1 replication system in the absence and presence of Vif_{HXB2} and Vif_{IIIB}

The ratio of white colonies to total colonies is defined as the population mutation frequency. The average number of G→A mutations per base pair in the 368-nt *prot-lacZα* construct is defined as the clone mutation frequency.

Reaction condition	Population mutation frequency	Clone mutation frequency ($\times 10^{-2}$)
A3G	0.87	2.2
A3G + Vif_{HXB2}	0.63[a]	0.9[a]
A3G + Vif_{IIIB}	0.90	1.5[b]

[a] Significant difference was designed as $p \leq 0.001$ *versus* A3G values.
[b] Significant difference was designed as $p \leq 0.01$ *versus* A3G values.

number of white colonies in the population (population mutation frequency) or the number of mutations per base pair (clone mutation frequency) (Table 2). We found that Vif_{HXB2} caused a significant decrease in both the population (1.4-fold) and clone mutation frequency (2-fold) from A3G alone (Table 2). The influence of Vif_{IIIB} was not as large with the population mutation frequency remaining the same as for A3G alone and the clone mutation frequency decreasing 1.5-fold (Table 2). Altogether, the data indicate that both Vif variants we tested can inhibit A3G-induced mutagenesis, consistent with previous results that tested Vif_{IIIB} (59) or Vif_{HXB2} (58). Furthermore, the effect of Vif_{HXB2} on A3G was more potent than Vif_{IIIB}, which is consistent with how these Vif variants function with respect to inducing degradation of A3G and other APOBEC3 enzymes (36).

Vif-mediated Inhibition of A3G Can Promote Sublethal Mutagenesis in a Model HIV-1 Replication System—Here we assessed the potential ability of each Vif variant to cause A3G to induce a sublethal amount of mutagenesis in the *prot* (supplemental Table S3). After determining the protease amino acid sequence of the mutated clones, we can infer whether the protease would retain activity or be inactivated by drawing on data from Loeb *et al.* (71) in which an extensive mutagenesis of the protease was conducted. Concomitant with the site to site decreases in mutation frequency (Table 1), we saw a decrease in the number of clones with amino acid changes of the protease in the presence of the Vif variants (supplemental Table S3).

When A3G-catalyzed deaminations occurred in the presence of Vif_{HXB2}, the types of mutations incurred were not changed but rather decreased with most mutations seen with A3G alone being absent in the presence of Vif_{HXB2} (supplemental Table S3). In the presence of Vif_{IIIB}, there were decreases in mutations at nine of the 13 sites mutated for A3G alone and changes in the mutation frequency, *i.e.* increased mutation or a novel site in four of the 13 sites mutated for A3G alone (supplemental Table S3). For example, the most heavily mutated site for native A3G is at amino acid 42 (Trp to stop; 44%). However, in the presence of Vif_{HXB2} and Vif_{IIIB}, the frequency of this mutation dropped to 0 and 16%, respectively (supplemental Table S3). It is interesting that some of the sites that were mutated only in the presence of Vif_{IIIB}, albeit at a low level, caused protease inhibitor resistance (4% for D30N and M46I; supplemental Table S3).

To determine whether each individual model provirus synthesized in our assay would code for an active or inactive protease, we analyzed each clone individually (Fig. 2). A3G-induced mutagenesis was able to cause inactivation of the *prot*

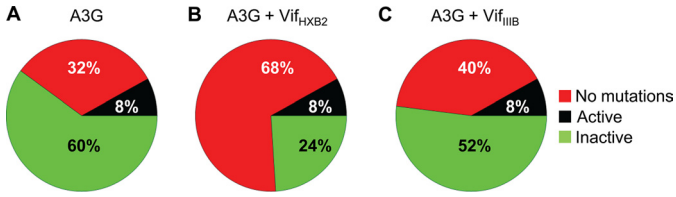

FIGURE 2. **Vif_{HXB2} and Vif_{IIIB} have a different effect on the decrease in A3G-induced mutations in the *prot* sequence.** Individual analysis of each *prot* clone enabled determination of the percentage of clones that would result in an unmutated (no mutations; *red*), mutated and active (*black*), or mutated and inactive (*green*) *prot*. *A*, A3G was able to inactivate the *prot* in 60% of clones and left an active *prot* in 8% of mutated clones. A3G did not induce any mutations in the *prot* in 32% of clones. *B*, A3G-induced mutagenesis in the presence of Vif_{HXB2} resulted in fewer mutations overall. There were 68% of clones with no mutations, 24% of clones were mutated and inactive, and 8% of clones were mutated but retained *prot* activity. *C*, the effect of Vif_{IIIB} on A3G-induced mutagenesis was less than that of Vif_{HXB2} and resulted in 40% of clones with no mutations, 52% of clones with inactive *prot*, and 8% of clones with mutated but active *prot*.

60% of the time and left the *prot* active only 8% of the time (Fig. 2*A*). A significant amount of clones (32%) had no mutations in the *prot* region. A3G-induced mutagenesis in the presence of Vif_{HXB2} changed this distribution so that 68% of clones had no mutations in the *prot* and 24% had mutations that inactivated the *prot* (Fig. 2*B*). Again, 8% of clones were mutated but still coded for an active *prot* (Fig. 2*B*). The same trend was found for A3G in the presence of Vif_{IIIB} where slightly more clones were not mutated (40%; Fig. 2*C*) in comparison with A3G alone (32%; Fig. 2*A*). These results are in agreement with the analysis of the total population of mutations (supplemental Table S3) where there was an overall decrease in mutations rather than an alteration of the mutational hot spots.

Vif Alters the Processive Scanning Mechanism of A3G—To investigate how Vif_{IIIB} and Vif_{HXB2} inhibit A3G-induced mutagenesis and why these variants differ in their effect (Fig. 1 and Tables 1 and 2), we conducted assays measuring A3G-catalyzed deaminations on synthetic DNA substrates. Specifically, the assay can measure the processive scanning behavior of A3G by using a 118-nt ssDNA substrate with two 5′-CCC deamination motifs spaced 61 nt apart (Fig. 3*A*, *schematic*). Fig. 3*A* shows a characteristic result of A3G in this assay. A3G deaminated both the 5′- and 3′-proximal CCC motifs, but there was a 2-fold preference for the 5′-motif due to an inherent catalytic orientation specificity of the active site (22). Of importance is the presence of a double deamination band, which indicates that a deamination occurred at both the 5′-C and 3′-C on the same ssDNA (Fig. 3*A*, *63 nt*). The processivity factor is calculated as a ratio of the intensity of this band to the calculated expected value of deaminations that would occur at both 5′- and 3′-proximal motifs if the enzyme were not processive (see "Experimental Procedures"). The processivity factor of 9.1 (Fig. 3*A*, *below gel*) means that A3G is 9 times more likely to undergo a processive deamination of both CCC motifs than to deaminate each of the motifs in separate enzyme-ssDNA encounters. Vif_{HXB2} and Vif_{IIIB} were able to decrease the processivity of A3G by at least 1.5-fold from 9.1 to 4.1 or 5.6, respectively (Fig. 3*A*).

To discern how the Vif variants are able to decrease the processivity of A3G, we used an assay that can make a distinction between the two scanning modes of A3G. A3G has been shown

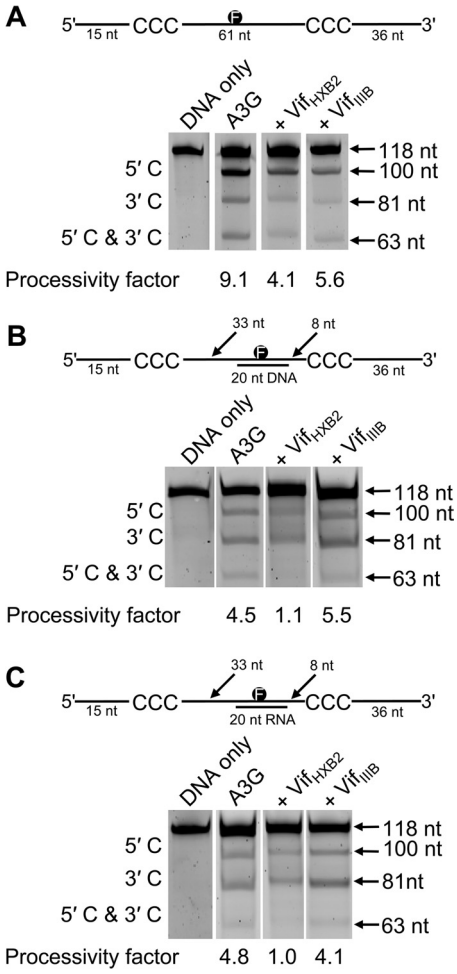

FIGURE 3. **Processivity of A3G in the absence and presence of Vif_{HXB2} and Vif_{IIIB}.** *A*, deamination of a 118-nt F-labeled ssDNA substrate by A3G. Two CCC motifs within the ssDNA sequence are spaced 61 nt apart. Single deaminations of the 5′-C and 3′-C were detected as the appearance of labeled 100- and 81-nt fragments, respectively; double deamination of both C residues on the same molecule resulted in a 63-nt labeled fragment (5′-C and 3′-C). A3G processivity was decreased by ~2-fold in the presence of Vif_{HXB2} (+*Vif_{HXB2}*) and Vif_{IIIB} (+*Vif_{IIIB}*). *B*, deamination of the substrate described for *A* but with a 20-nt ssDNA annealed between the two CCC motifs that can block the sliding component of A3G processivity. This resulted in a 2-fold decrease in A3G processivity. Processive deaminations were still observed due to the jumping component of A3G processive movement. In the presence of Vif_{HXB2}, the processivity of A3G was nearly absent, indicating that the jumping component of A3G has been inhibited. This is in contrast to the Vif_{IIIB}, which had no effect on A3G jumping movement. *C*, deamination of the substrate described for *B* but with a 20-nt RNA annealed between the two CCC motifs. Processive scanning of A3G on this substrate in the absence and presence of Vif_{HXB2} and Vif_{IIIB} was similar to that observed for *B*. The measurements of processivity (*Processivity factor*) are shown *below* the gel. Values are an average from at least three independent experiments, and the S.D. for the processivity factors are as follows: in *A*, A3G, 1.90; +Vif_{HXB2}, 0.03; +Vif_{IIIB}, 0.65; in *B*, A3G, 0.80; +Vif_{HXB2}, 0.20; +Vif_{IIIB}, 0.76; in *C*, A3G, 1.20; +Vif_{HXB2}, 0.16; +Vif_{IIIB}, 0.40.

to scan ssDNA by sliding and microscopic dissociations and reassociations termed jumping (12, 19). This bifunctional processive mode was identified using an experiment where a complementary DNA oligonucleotide was annealed between two CCC motifs on an ssDNA substrate (Fig. 3*B*, *schematic*). The partially dsDNA to which the enzyme cannot effectively bind acts as a block to the sliding component of A3G processivity (12, 72). However, A3G can still transverse the block by jumping. As such, A3G incurred a ~2-fold decrease in processivity (Fig. 3, compare *A* and *B*, processivity factors of 9.1 and 4.5,

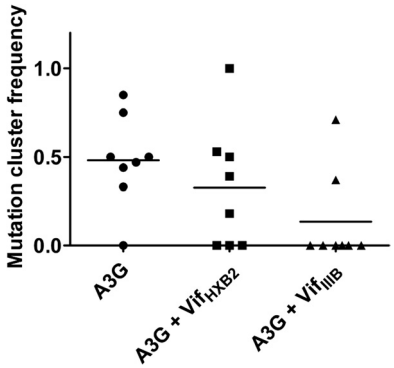

FIGURE 4. **Mutation cluster frequency of A3G is decreased in the presence of Vif_{IIIB} but not Vif_{HXB2}.** Sliding movement of A3G is inferred from clustered mutations. The frequency of clustered mutations was scored in eight regions of the *prot-lacZα* that contain three to six G residues. *Horizontal bars* represent the average mutation cluster frequency. The data show that A3G alone and in the presence of Vif_{HXB2} induced a similar frequency of clustered mutations (*p* value, 0.32). However, A3G in the presence of Vif_{IIIB} induced significantly fewer clustered mutations (*p* value, 0.02).

respectively). When Vif_{HXB2} was added to the reaction with the partially dsDNA substrate, the processivity factor of A3G decreased another 2-fold from 4.1 to 1.1 (Fig. 3, *A* and *B*, *Processivity factor*), and there was a visible decrease of the double deaminations to almost none (Fig. 3*B*, *63 nt*). This indicates that Vif_{HXB2} can inhibit the jumping component of A3G so that it is no longer able to transverse the dsDNA. A3G was still able to slide because processive deaminations occurred on fully ssDNA (Fig. 3*A*). Vif_{IIIB} did not affect the ability of A3G to jump because the processivity factor in the presence of the dsDNA is 5.5 (Fig. 3*B*, *Processivity factor*), which is similar to the processivity of A3G in the presence of Vif_{IIIB} on fully ssDNA (processivity factor of 5.6; Fig. 3*A*). However, Vif_{IIIB} does appear to affect A3G processivity because it decreased the processivity factor on ssDNA 1.5-fold (processivity factor decreased from 9.1 to 5.6; Fig. 3*A*), suggesting that Vif_{IIIB} may inhibit A3G sliding. Similar results were found when we used a complimentary RNA oligonucleotide as a block (Fig. 3*C*). An RNA/DNA hybrid block would be what A3G encounters on HIV-1 (−)DNA during viral replication and suggests that the decrease in A3G-induced mutagenesis seen in the HIV-1 replication assay (Fig. 1) was due to a partial inhibition of A3G processivity by the Vif variants (Fig. 3, *A*–*C*).

To further test this hypothesis, we examined the sequences of clones from the HIV-1 replication assay. We can analyze the spatial proximity of mutations in the clones and relate it to processivity where clustered mutations are indicative of scanning by local sliding and distantly spaced singleton mutations are indicative of scanning by jumping (19). Areas of the 368-nt (+)DNA sequence (containing *prot* and *lacZα*), which contains multiple G residues, were used to analyze the frequency of clustered A3G-induced G→A mutations. If the sliding component of A3G ssDNA scanning mechanism is retained, A3G should be able to induce mutagenesis at multiple G residues in a close region, *i.e.* 10 nt or less. The mean clustered mutation frequency for A3G alone (0.48; Fig. 4) is similar to that for the situation when Vif_{HXB2} was present (0.33; *p* value, 0.32; Fig. 4). These data are consistent with Fig. 3, *A*–*C*, which shows that A3G retained the ability to slide, but not jump, in the presence

TABLE 3

Apparent dissociation constants (K_d) of A3G, D128K, and Vif variants

The apparent K_d values are shown with the S.D. that was calculated from three independent experiments. No value indicates that the experiment was not conducted.

Enzyme	Apparent dissociation constant (K_d)			
	F-A3G	F-D128K	*prot* (−)ssDNA	118-nt ssDNA
			nM	
A3G			270 ± 59	203 ± 18
D128K				183 ± 13
Vif_{HXB2}	90 ± 15	No binding detected	27 ± 1	67 ± 18
Vif_{IIIB}	78 ± 10	No binding detected	92 ± 13	79 ± 15
A3G + Vif_{HXB2}				158 ± 20
A3G + Vif_{IIIB}				135 ± 11
D128K + Vif_{HXB2}				72 ± 10
D128K + Vif_{IIIB}				51 ± 19

of Vif_{HXB2}. In the presence of Vif_{IIIB}, A3G was less capable of inducing mutations that are closely spaced (0.14; *p* value, 0.02; Fig. 4). This indicates that A3G was less able to scan ssDNA by sliding when Vif_{IIIB} was present and is in agreement with processivity data obtained from synthetic substrates (Fig. 3, *A–C*).

Inhibitory Mechanism of Vif Is Mediated by an Interaction with A3G—A3G is known to physically interact with Vif (30–32), which suggests that Vif could alter the processivity of A3G through a protein-protein interaction. That the two Vif variants affected A3G processivity differently supports this notion (Figs. 3 and 4). To investigate this possibility, we used the A3G D128K mutant (referred to as D128K), which is insensitive to Vif-mediated degradation and has been shown to have a disrupted physical interaction with Vif (42–44, 73–75). Our rotational anisotropy data confirm the previous findings as we found no detectable interaction between F-D128K and the Vif variants (Table 3). However, we found that Vif_{HXB2} and Vif_{IIIB} interacted similarly with F-A3G. The measured apparent K_d values of 90 nM (Vif_{HXB2}) and 78 nM (Vif_{IIIB}) for F-A3G indicate that a strong interaction can occur between these proteins (Table 3).

We tested the ability of D128K to induce mutations in a model HIV-1 replication system in the absence and presence of the Vif variants. The mutational spectrum for D128K alone shows peaks for highly mutated sites in the same locations as for A3G (compare Fig. 1*A* and Fig. 5*A*). The intensity of the mutations among the sites differed slightly likely because of the stochastic nature of A3G deamination (18). The mutation frequencies are nearly identical for D128K and A3G at the population level (D128K, 0.96 (Table 4); A3G, 0.87 (Table 2)) and clone level (D128K, 2.2×10^{-2} (Table 4); A3G, 2.2×10^{-2} (Table 2)). Overall, the results are consistent with D128K behaving similarly to A3G in this assay. When both Vif_{IIIB} and Vif_{HXB2} were added to the reaction with D128K, we observed no decrease in the mutagenic ability of D128K (Fig. 5, *A–F*, and Table 4) in contrast to A3G (Fig. 1, *A–F*, and Table 2). In addition, we found no effects on D128K processive scanning by sliding by the addition of Vif_{HXB2} or Vif_{IIIB} to the model HIV-1 replication assay as the mutation cluster frequency (Fig. 6) and frequency of mutations (Fig. 5 and Table 4) remained constant in all three experimental conditions. This observation is in agreement with data obtained on the 118-nt substrate where neither Vif_{HXB2} nor Vif_{IIIB} was found to change D128K processivity (data not shown). Altogether, the data support a model in which an alteration in the processivity of A3G in the presence of Vif is caused by a Vif-A3G interaction.

Vif Affects the Specific Activity of A3G and D128K—Despite evidence that a Vif-A3G interaction was responsible for the observed decrease in A3G-induced mutagenesis (Table 3 and compare Figs. 5 and 1), Vif has been shown to bind DNA and RNA molecules (54, 76, 77). Therefore, we assessed whether the Vif variants could additionally alter A3G deamination activity, *i.e.* decrease specific activity, by binding to the ssDNA substrate. Rotational anisotropy data show that A3G could bind to the substrate used in the processivity assays (Fig. 3*A*, 118-nt substrate) with an apparent K_d of 203 nM (Table 3), which is ~3-fold higher than the apparent K_d values of the Vif variants for this substrate (K_d of Vif_{HXB2}, 67 nM; K_d of Vif_{IIIB}, 79 nM; Table 3). We also examined the binding of A3G and Vif to the *prot* (−)DNA, which was part of the deamination substrate for the HIV-1 replication assay (Fig. 1). We observed A3G binding to the *prot* (−)DNA with an apparent K_d of 270 nM (Table 3), which is 10-fold (K_d of Vif_{HXB2}, 27 nM; Table 3) and 3-fold (K_d of Vif_{IIIB}, 92 nM; Table 3) higher than the binding of Vif variants to this substrate. Therefore, in both our experimental systems, the apparent K_d values of Vif for DNA and F-A3G (K_d of F-A3G from Vif_{HXB2} and Vif_{IIIB}, 90 and 78 nM, respectively; Table 3) are similar, suggesting the possibility that Vif could compete with A3G for the ssDNA substrate and decrease the specific activity of A3G.

To test this hypothesis, we used D128K, which does not interact with Vif (Table 3). There was no effect of Vif on D128K-induced mutagenesis (Fig. 5), suggesting that Vif interactions with the DNA in the HIV-1 replication assay are inconsequential with regard to processivity (Fig. 6). Notwithstanding, a decrease in specific activity could be occurring but cannot be observed in the HIV-1 replication assay because deamination events are dependent on and limited by other factors such as the rates of RNA degradation and (+)DNA synthesis. To determine whether Vif can decrease the specific activity of A3G or D128K, we used the 118-nt ssDNA substrate used previously for the processive deamination assay (Fig. 3*A*). The experiment involved preincubation of Vif and D128K or A3G together, and then the reaction was started by the addition of the 118-nt ssDNA substrate. On the 118-nt ssDNA substrate, D128K had a 4-fold higher specific activity (40 pmol/μg/min; Table 5) than A3G (10 pmol/μg/min; Table 5). However, Vif (HXB2 and IIIB) can decrease D128K specific activity 80-fold (D128K + Vif_{HXB2}, 0.5 pmol/μg/min; Table 5) or 50-fold (D128K + Vif_{IIIB},0.8 pmol/μg/min; Table 5) in comparison with an 8-fold (A3G + Vif_{HXB2}, 1.2 pmol/μg/min; Table 5) or 6-fold (A3G + Vif_{IIIB}, 1.8 pmol/μg/min; Table 5) decrease in A3G activity. These data suggest that there was a significant amount of Vif binding to the 118-nt ssDNA substrate in the presence of D128K, causing a large decrease in specific activity. To investigate this further, we determined the apparent K_d of a D128K and Vif_{HXB2} mixture and found that the value (K_d of 72 nM; Table 3) was almost identical to that of Vif_{HXB2} alone (K_d of 67 nM; Table 3). These data support the hypothesis that Vif has a dominant role in ssDNA binding in the presence of D128K that had an ~3-fold higher apparent K_d than Vif (K_d of 183 nM; Table 3). Similar results were found with a D128K and Vif_{IIIB}

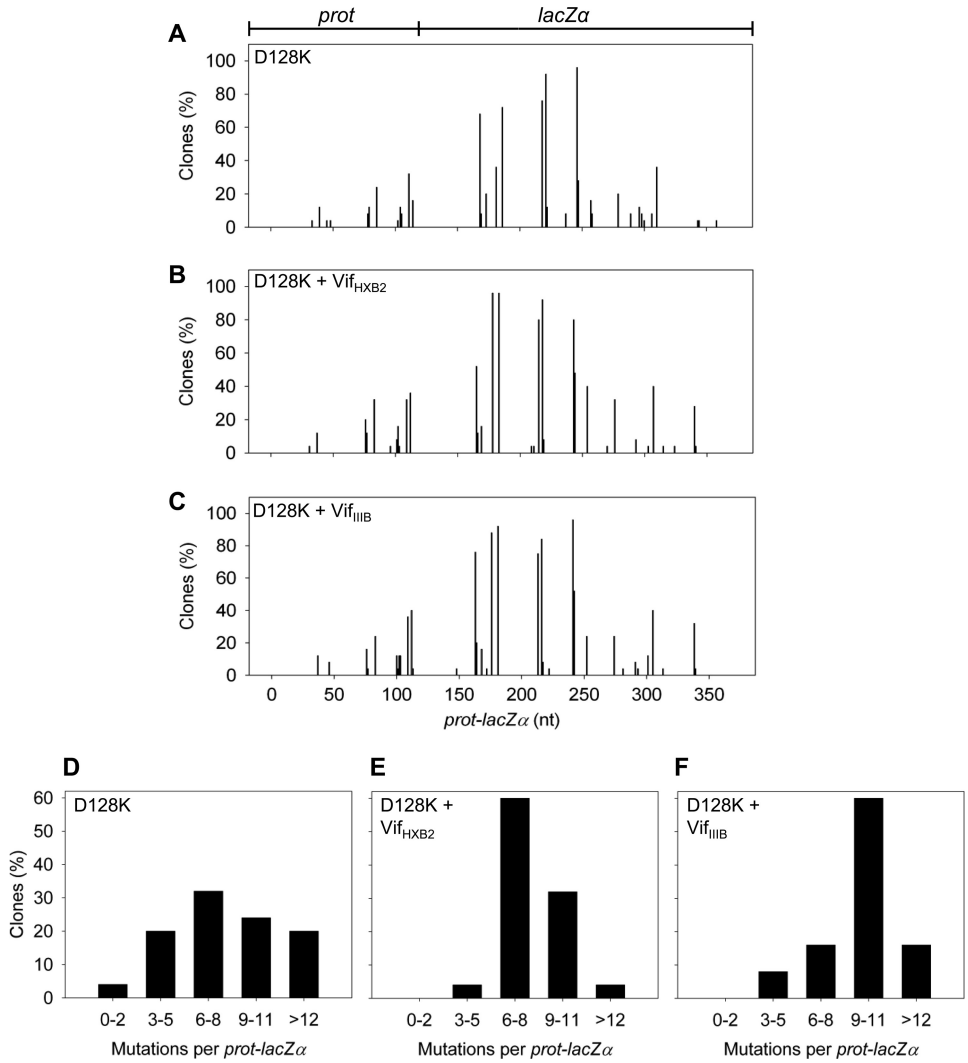

FIGURE 5. **A3G D128K-induced mutagenesis is unaffected by Vif$_{HXB2}$ and Vif$_{IIIB}$ in a model HIV-1 replication system.** *A–C,* spectra of mutations incurred in the 368-nt *prot-lacZα* construct are plotted as the percentage of clones containing a mutation at a particular location (nt) for D128K (*A*), D128K in the presence of Vif$_{HXB2}$ (*B*), and D128K in the presence of Vif$_{IIIB}$ (*C*). *D–F,* histograms illustrate that the population distribution of mutations per *prot-lacZα* construct for D128K (*D*) was not decreased in the presence of Vif$_{HXB2}$ (*E*) or Vif$_{IIIB}$ (*F*).

TABLE 4

D128K-mediated mutation frequencies in a model HIV-1 replication system in the absence and presence of Vif$_{HXB2}$ and Vif$_{IIIB}$

The ratio of white colonies to total colonies is defined as the population mutation frequency. The average number of G→A mutations per base pair in the 368-nt *prot-lacZα* construct is defined as the clone mutation frequency.

Reaction condition	Population mutation frequency	Clone mutation frequency ($\times 10^{-2}$)
D128K	0.96	2.2
D128K + Vif$_{HXB2}$	0.93	2.3
D128K + Vif$_{IIIB}$	0.90	2.6[a]

[a] Significant difference was designed as $p \leq 0.05$ *versus* D128K values.

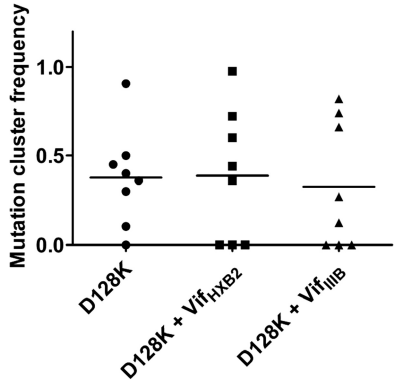

FIGURE 6. **Vif$_{IIIB}$ and Vif$_{HXB2}$ do not decrease the mutation cluster frequency of D128K.** Shown is the analysis of sequenced clones obtained from the HIV-1 replication assay conducted for D128K in the absence and presence of Vif$_{HXB2}$ and Vif$_{IIIB}$. The frequency of clustered mutations was scored in eight regions of the *prot-lacZα* that contain three to six G residues. Inferred sliding movement from clustered mutations was unchanged by the presence of Vif$_{HXB2}$ or Vif$_{IIIB}$. *Horizontal bars* represent the average mutation cluster frequency. The data show that D128K alone and in the presence of Vif$_{HXB2}$ or Vif$_{IIIB}$ induced a similar frequency of clustered mutations (*p* value, 0.96 and 0.75, respectively).

mixture binding to the 118-nt ssDNA substrate (K_d of 51 nM; Table 3). In contrast, an A3G and Vif$_{HXB2}$ or A3G and Vif$_{IIIB}$ complex had an apparent K_d (A3G and Vif$_{HXB2}$, K_d of 158 nM; A3G and Vif$_{IIIB}$, K_d of 135 nM; Table 3) that was higher than that of Vif$_{HXB2}$ or Vif$_{IIIB}$ alone (Vif$_{HXB2}$, K_d of 67 nM; Vif$_{IIIB}$, K_d of 79 nM; Table 3). Based on these data, it appears that Vif molecules that interact with A3G may not be able to bind the ssDNA substrate efficiently through the Vif DNA binding domain because it is near the A3G interaction residues (78). This would

TABLE 5

Specific activities of A3G and D128K in the absence and presence of Vif variants

The specific activity was determined using the 118-nt ssDNA substrate, and the values are shown with the S.D. that was calculated from three independent experiments.

Reaction condition	Specific activity
	pmol/μg/min
A3G	10 ± 0.3
A3G + Vif_{HXB2}	1.2 ± 0.3
A3G + Vif_{IIIB}	1.8 ± 0.9
D128K	40 ± 9
D128K + Vif_{HXB2}	0.5 ± 0.2
D128K + Vif_{IIIB}	0.8 ± 0.4

lower the effective DNA binding concentration of Vif and result in an increase in the apparent K_d value (Table 3). However, the Vif variants may still contact the ssDNA because the apparent K_d values of the Vif·A3G complex are slightly less than that of A3G alone (K_d of 203 nM; Table 3).

In contrast to A3G, which had a decrease in processivity in the presence of Vif (Figs. 3 and 4), we did not observe a decrease in D128K processivity on the 118-nt substrate (data not shown) or in the HIV-1 replication assay (Figs. 5 and 6) in the presence of the Vif variants despite the decrease in specific activity (Table 5). Together with binding data (Table 3), the results indicate that Vif can bind ssDNA and compete with D128K for substrate access, which results in a decrease in D128K specific activity (Table 5). This activity was lessened in the presence of A3G (Table 5), which bound Vif with high affinity (Table 3). Therefore, the data support a model in which the inhibition of processivity and specific activity by Vif are two different functions mediated by an A3G-Vif or ssDNA-Vif interaction, respectively.

DISCUSSION

Although Vif induces polyubiquitination and degradation of A3G in HIV-1 infected cells (29–32), the clearance of A3G from the host cell may not be complete (55, 56). Vif can use alternate ways of inhibiting A3G activity such as suppressing A3G mRNA translation, blocking virus encapsidation of A3G, and inhibiting A3G deamination activity (41, 45–47, 58, 59). Here we examined the mechanism by which Vif can inhibit A3G deamination activity.

Our data demonstrate that Vif changes the processive scanning mechanism of A3G (Figs. 3 and 4), and this appears to account for the observed decrease in A3G-induced mutagenesis occurring in a model HIV-1 replication system (Fig. 1). The data indicate that the change in A3G processivity by the Vif variants is due to a protein-protein interaction because A3G D128K-induced mutagenesis was unaffected by Vif (Fig. 5). The implications of the data are that any residual A3G that escapes Vif-mediated degradation and becomes encapsidated into HIV-1 virions in the presence of Vif is likely to be ineffective at restricting HIV-1 replication (55, 56). Vif and A3G co-encapsidation could also be induced by a therapeutic option that prevents Vif interaction with ubiquitin ligase components but retains Vif interaction with A3G (61). Of note, while this work was being completed, it was discovered that core binding factor-β stabilizes Vif in cells (37, 38). We confirmed that a core binding factor-β·Vif complex affects A3G processivity and specific activity similarly to the GST-Vif used in our study (supplemental Fig. S2, supplemental Table S4, and supplemental Experimental Procedures), which provides additional evidence that Vif is likely to affect A3G deamination ability *in vivo*.

The results of the model HIV-1 replication assay for A3G (Figs. 1 and 4) and D128K (Figs. 5 and 6) in the presence of the Vif variants support a model in which a Vif·A3G complex results in a decreased ability of A3G to deaminate C→U processively, resulting in a decrease in mutagenesis. However, we examined whether there were additional effects caused by Vif binding ssDNA. We reasoned that the ssDNA binding effects of Vif would manifest as a decrease in specific activity of A3G or D128K due to competition for substrate binding. This cannot be observed in the HIV-1 replication assay because substrate access is limited by RNA degradation and (+)DNA synthesis. Although this alone argues that the inhibition of A3G processivity by Vif is of primary importance, we examined the effect of Vif binding a synthetic ssDNA substrate to fully characterize the mechanisms by which Vif can affect A3G deamination activity. We hypothesized that because the residues of Vif that interact with A3G are near the Vif RNA/DNA binding domain (78) the Vif·A3G complex may contact ssDNA more efficiently through A3G DNA binding residues. This would argue that there is a minimal effect of Vif on A3G specific activity. The observed smaller decrease in A3G specific activity (6–8-fold; Table 5) than in D128K specific activity (50–80-fold; Table 5) in the presence of the Vif variants is consistent with the model. As such, our data are in agreement with previously published literature that Vif can decrease A3G deamination activity (58, 59), but here we found that the mechanism by which this occurs involves Vif affecting primarily the processive scanning (Figs. 3, *A–C*, and 4) rather than the specific activity (Table 5) of A3G. This is also supported by rotational anisotropy data showing that Vif variants bound ssDNA with the same apparent K_d in the absence or presence of D128K but had an increase in the apparent K_d in the presence of A3G (Table 3). Based on the data obtained with D128K for which we observed a decrease in specific activity (Table 5) but not processivity (Figs. 5 and 6), it appears that these two inhibitory functions are implemented by free Vif and A3G-bound Vif, respectively (Tables 3 and 5). The Vif-bound A3G did not efficiently induce mutagenesis of (−)DNA (Figs. 1, *A–C*, and 2), suggesting that both processive jumping and sliding movements are required in agreement with a previous report (19).

Vif is known to physically interact with A3G, and Asp^{128} is a key residue that mediates this interaction (42). The Asp^{128} is predicted to be located on loop 7 of the N-terminal half of A3G (supplemental Fig. S1). The predicted loop 7 is functionally important because the amino acids $^{124}YYFW^{127}$ located in this region mediate virion incorporation (26, 27), oligomerization (22, 26), and the jumping component of A3G processivity (19). The proximity of Asp^{128} to the key processivity residues, $^{126}FW^{127}$, which mediate A3G jumping movements (19), provides a logical explanation of how Vif_{HXB2} can block the jumping ability of A3G (Fig. 3, *A–C*). Together with the high affinity of A3G for binding Vif_{HXB2} (Table 3), the data support that Vif_{HXB2} inhibition of A3G deamination ability is primarily through a protein-protein interaction. It has been demon-

strated that a loss of jumping ability in the A3G F126A/W127A mutant results in a large decrease of A3G-induced mutations in the HIV-1 replication assay (19), and we observed the same phenomenon here (Fig. 1, *A* and *B* and *D* and *E*). The decreased mutagenesis observed in the HIV-1 replication assay is likely to correlate with a decrease in HIV-1 infectivity because virion-encapsidated F126L or W127A mutants are less effective at restricting HIV-1 in single cycle infectivity assays (27). We have hypothesized that this is because A3G requires the jumping component of its processive mechanism to effectively transverse the RNA/DNA hybrid regions left by RT RNase H activity (19). In the presence of Vif_{HXB2}, A3G was capable of sliding (Fig. 4), but any surrounding RNA/DNA hybrid regions would essentially lock the A3G into an isolated area of (−)DNA. Because of the extended residence time A3G has on ssDNA, a half-life of ~4 min (72), remaining in a confined (−)DNA region would result in an ineffective search over the whole (−)DNA (Fig. 1, compare *A* and *B* and *D* and *E*).

Interestingly, Vif_{IIIB} had a different effect on A3G processivity than Vif_{HXB2} and inhibited A3G sliding (Figs. 3, *A–C*, and 4). Based on phylogenic analysis, Vif_{IIIB} is less similar to Vif_{HXB2} than other variants such as Vif_{ELI-1} or Vif_{YU-2} (supplemental Fig. S3), providing a rationale for the difference in their effect on A3G and suggesting that the inhibition of A3G jumping rather than sliding is more likely to be observed in other variants. It has been reported that the sliding component of A3G is mediated by helix 6 (19). Helix 6 is predicted to be adjacent to loop 7 (supplemental Fig. S1). The contacts of Vif with A3G have been shown to encompass ^{128}DPD^{130} on loop 7 and hypothesized to also extend beyond loop 7 (73), which is supported by a mutagenesis study (79). Random mutagenesis identified residues in the N-terminal domain predicted helices 3, 4, and 6 and predicted loops 1 and 3 that interact with Vif_{IIIB} (79). This may be due to a charged surface on A3G that interacts with Vif through multiple structural components. This appears to be the case for A3F, which interacts with Vif through its C-terminal half where a negatively charged surface surrounding predicted C-terminal helices 2, 3, and 4 may interact with Vif in addition to a key residue, Glu^{324} (80–82). These reports provide a supporting rationale for how A3G sliding, which is mediated by helix 6 (19), could be affected in our study by Vif_{IIIB}. Furthermore, Vif_{IIIB} and Vif_{HXB2} have been found to differentially mediate the extent of APOBEC3 enzyme degradation (36), which implies they may interact with A3G differently beyond residues ^{128}DPD^{130}. Because A3G and Vif_{IIIB} interacted with high affinity (K_d of 78 nM; Table 3), the data support the conclusion that Vif_{IIIB} inhibition of A3G activity is primarily through a protein-protein interaction that disrupts the sliding component of the processive ssDNA scanning mechanism.

It has been reported previously that any type of small molecules that could be designed to bind A3G and block its interaction with Vif may not be a relevant therapeutic option if A3G functions imparted by the residues adjacent to Asp^{128} such as virion encapsidation are also affected (60, 73). For this reason, alternate therapeutic options have been put forward such as small molecules that bind Vif (83) or the ubiquitin ligase complex (61) to inhibit degradation of A3G. The latter therapeutic option would presumably allow a maintained interaction between Vif and A3G. Based on our data, a therapeutic option that left Vif in the cell, allowing it to form a Vif·A3G complex, would not enable virion-encapsidated Vif·A3G to reliably restrict HIV-1 replication (Figs. 1, *A–F*, and 2). Because the number of A3G mutations has been correlated with HIV-1 inactivation (55, 84), an implication of our results is that the Vif·A3G complex could lead to sublethal mutagenesis of HIV-1.

REFERENCES

1. Sheehy, A. M., Gaddis, N. C., Choi, J. D., and Malim, M. H. (2002) Isolation of a human gene that inhibits HIV-1 infection and is suppressed by the viral Vif protein. *Nature* **418,** 646–650
2. Mangeat, B., Turelli, P., Caron, G., Friedli, M., Perrin, L., and Trono, D. (2003) Broad antiretroviral defence by human APOBEC3G through lethal editing of nascent reverse transcripts. *Nature* **424,** 99–103
3. Harris, R. S., Bishop, K. N., Sheehy, A. M., Craig, H. M., Petersen-Mahrt, S. K., Watt, I. N., Neuberger, M. S., and Malim, M. H. (2003) DNA deamination mediates innate immunity to retroviral infection. *Cell* **113,** 803–809
4. Zhang, H., Yang, B., Pomerantz, R. J., Zhang, C., Arunachalam, S. C., and Gao, L. (2003) The cytidine deaminase CEM15 induces hypermutation in newly synthesized HIV-1 DNA. *Nature* **424,** 94–98
5. Strebel, K., and Khan, M. A. (2008) APOBEC3G encapsidation into HIV-1 virions: which RNA is it? *Retrovirology* **5,** 55
6. Suspène, R., Sommer, P., Henry, M., Ferris, S., Guétard, D., Pochet, S., Chester, A., Navaratnam, N., Wain-Hobson, S., and Vartanian, J. P. (2004) APOBEC3G is a single-stranded DNA cytidine deaminase and functions independently of HIV reverse transcriptase. *Nucleic Acids Res.* **32,** 2421–2429
7. Yu, Q., König, R., Pillai, S., Chiles, K., Kearney, M., Palmer, S., Richman, D., Coffin, J. M., and Landau, N. R. (2004) Single-strand specificity of APOBEC3G accounts for minus-strand deamination of the HIV genome. *Nat. Struct. Mol. Biol.* **11,** 435–442
8. Coffin, J. M., Hughes, S. H., and Varmus, H. E. (1997) *Retroviruses*, pp. 121–160, Cold Spring Harbor Laboratory Press, Cold Spring Harbor, NY
9. Rausch, J. W., and Le Grice, S. F. (2004) 'Binding, bending and bonding': polypurine tract-primed initiation of plus-strand DNA synthesis in human immunodeficiency virus. *Int. J. Biochem. Cell Biol.* **36,** 1752–1766
10. Hu, C., Saenz, D. T., Fadel, H. J., Walker, W., Peretz, M., and Poeschla, E. M. (2010) The HIV-1 central polypurine tract functions as a second line of defense against APOBEC3G/F. *J. Virol.* **84,** 11981–11993
11. Suspène, R., Rusniok, C., Vartanian, J. P., and Wain-Hobson, S. (2006) Twin gradients in APOBEC3 edited HIV-1 DNA reflect the dynamics of lentiviral replication. *Nucleic Acids Res.* **34,** 4677–4684
12. Chelico, L., Pham, P., Calabrese, P., and Goodman, M. F. (2006) APOBEC3G DNA deaminase acts processively 3′ → 5′ on single-stranded DNA. *Nat. Struct. Mol. Biol.* **13,** 392–399
13. von Hippel, P. H., and Berg, O. G. (1989) Facilitated target location in biological systems. *J. Biol. Chem.* **264,** 675–678
14. Stanford, N. P., Szczelkun, M. D., Marko, J. F., and Halford, S. E. (2000) One- and three-dimensional pathways for proteins to reach specific DNA sites. *EMBO J.* **19,** 6546–6557
15. Halford, S. E., and Marko, J. F. (2004) How do site-specific DNA-binding proteins find their targets? *Nucleic Acids Res.* **32,** 3040–3052
16. Senavirathne, G., Jaszczur, M., Auerbach, P. A., Upton, T. G., Chelico, L., Goodman, M. F., and Rueda, D. (2012) Single-stranded DNA scanning and deamination by APOBEC3G cytidine deaminase at single molecule resolution. *J. Biol. Chem.* **287,** 15826–15835
17. Shlyakhtenko, L. S., Lushnikov, A. Y., Miyagi, A., Li, M., Harris, R. S., and Lyubchenko, Y. L. (2012) Nanoscale structure and dynamics of ABOBEC3G complexes with single-stranded DNA. *Biochemistry* **51,** 6432–6440
18. Chelico, L., Pham, P., and Goodman, M. F. (2009) Stochastic properties of processive cytidine DNA deaminases AID and APOBEC3G. *Philos. Trans. R. Soc. Lond. B Biol. Sci.* **364,** 583–593
19. Feng, Y., and Chelico, L. (2011) Intensity of deoxycytidine deamination of HIV-1 proviral DNA by the retroviral restriction factor APOBEC3G is mediated by the noncatalytic domain. *J. Biol. Chem.* **286,** 11415–11426

20. Haché, G., Liddament, M. T., and Harris, R. S. (2005) The retroviral hypermutation specificity of APOBEC3F and APOBEC3G is governed by the C-terminal DNA cytosine deaminase domain. *J. Biol. Chem.* **280,** 10920–10924
21. Navarro, F., Bollman, B., Chen, H., König, R., Yu, Q., Chiles, K., and Landau, N. R. (2005) Complementary function of the two catalytic domains of APOBEC3G. *Virology* **333,** 374–386
22. Chelico, L., Prochnow, C., Erie, D. A., Chen, X. S., and Goodman, M. F. (2010) Structural model for deoxycytidine deamination mechanisms of the HIV-1 inactivation enzyme APOBEC3G. *J. Biol. Chem.* **285,** 16195–16205
23. Wedekind, J. E., Gillilan, R., Janda, A., Krucinska, J., Salter, J. D., Bennett, R. P., Raina, J., and Smith, H. C. (2006) Nanostructures of APOBEC3G support a hierarchical assembly model of high molecular mass ribonucleoprotein particles from dimeric subunits. *J. Biol. Chem.* **281,** 38122–38126
24. Bennett, R. P., Salter, J. D., Liu, X., Wedekind, J. E., and Smith, H. C. (2008) APOBEC3G subunits self-associate via the C-terminal deaminase domain. *J. Biol. Chem.* **283,** 33329–33336
25. McDougall, W. M., Okany, C., and Smith, H. C. (2011) Deaminase activity on single-stranded DNA (ssDNA) occurs *in vitro* when APOBEC3G cytidine deaminase forms homotetramers and higher-order complexes. *J. Biol. Chem.* **286,** 30655–30661
26. Huthoff, H., Autore, F., Gallois-Montbrun, S., Fraternali, F., and Malim, M. H. (2009) RNA-dependent oligomerization of APOBEC3G is required for restriction of HIV-1. *PLoS Pathog.* **5,** e1000330
27. Bulliard, Y., Turelli, P., Röhrig, U. F., Zoete, V., Mangeat, B., Michielin, O., and Trono, D. (2009) Functional analysis and structural modeling of human APOBEC3G reveal the role of evolutionarily conserved elements in the inhibition of human immunodeficiency virus type 1 infection and Alu transposition. *J. Virol.* **83,** 12611–12621
28. Sheehy, A. M., Gaddis, N. C., and Malim, M. H. (2003) The antiretroviral enzyme APOBEC3G is degraded by the proteasome in response to HIV-1 Vif. *Nat. Med.* **9,** 1404–1407
29. Yu, X., Yu, Y., Liu, B., Luo, K., Kong, W., Mao, P., and Yu, X. F. (2003) Induction of APOBEC3G ubiquitination and degradation by an HIV-1 Vif-Cul5-SCF complex. *Science* **302,** 1056–1060
30. Stopak, K., de Noronha, C., Yonemoto, W., and Greene, W. C. (2003) HIV-1 Vif blocks the antiviral activity of APOBEC3G by impairing both its translation and intracellular stability. *Mol. Cell* **12,** 591–601
31. Marin, M., Rose, K. M., Kozak, S. L., and Kabat, D. (2003) HIV-1 Vif protein binds the editing enzyme APOBEC3G and induces its degradation. *Nat. Med.* **9,** 1398–1403
32. Conticello, S. G., Harris, R. S., and Neuberger, M. S. (2003) The Vif protein of HIV triggers degradation of the human antiretroviral DNA deaminase APOBEC3G. *Curr. Biol.* **13,** 2009–2013
33. Bishop, K. N., Holmes, R. K., Sheehy, A. M., Davidson, N. O., Cho, S. J., and Malim, M. H. (2004) Cytidine deamination of retroviral DNA by diverse APOBEC proteins. *Curr. Biol.* **14,** 1392–1396
34. Zennou, V., and Bieniasz, P. D. (2006) Comparative analysis of the antiretroviral activity of APOBEC3G and APOBEC3F from primates. *Virology* **349,** 31–40
35. Chaipan, C., Smith, J. L., Hu, W. S., and Pathak, V. K. (2013) APOBEC3G restricts HIV-1 to a greater extent than APOBEC3F and APOBEC3DE in human primary CD4+ T cells and macrophages. *J. Virol.* **87,** 444–453
36. Marin, M., Golem, S., Rose, K. M., Kozak, S. L., and Kabat, D. (2008) Human immunodeficiency virus type 1 Vif functionally interacts with diverse APOBEC3 cytidine deaminases and moves with them between cytoplasmic sites of mRNA metabolism. *J. Virol.* **82,** 987–998
37. Jäger, S., Kim, D. Y., Hultquist, J. F., Shindo, K., LaRue, R. S., Kwon, E., Li, M., Anderson, B. D., Yen, L., Stanley, D., Mahon, C., Kane, J., Franks-Skiba, K., Cimermancic, P., Burlingame, A., Sali, A., Craik, C. S., Harris, R. S., Gross, J. D., and Krogan, N. J. (2012) Vif hijacks CBF-β to degrade APOBEC3G and promote HIV-1 infection. *Nature* **481,** 371–375
38. Zhang, W., Du, J., Evans, S. L., Yu, Y., and Yu, X. F. (2012) T-cell differentiation factor CBF-β regulates HIV-1 Vif-mediated evasion of host restriction. *Nature* **481,** 376–379
39. Mehle, A., Strack, B., Ancuta, P., Zhang, C., McPike, M., and Gabuzda, D. (2004) Vif overcomes the innate antiviral activity of APOBEC3G by promoting its degradation in the ubiquitin-proteasome pathway. *J. Biol. Chem.* **279,** 7792–7798
40. Iwatani, Y., Chan, D. S., Liu, L., Yoshii, H., Shibata, J., Yamamoto, N., Levin, J. G., Gronenborn, A. M., and Sugiura, W. (2009) HIV-1 Vif-mediated ubiquitination/degradation of APOBEC3G involves four critical lysine residues in its C-terminal domain. *Proc. Natl. Acad. Sci. U.S.A.* **106,** 19539–19544
41. Mariani, R., Chen, D., Schröfelbauer, B., Navarro, F., König, R., Bollman, B., Münk, C., Nymark-McMahon, H., and Landau, N. R. (2003) Species-specific exclusion of APOBEC3G from HIV-1 virions by Vif. *Cell* **114,** 21–31
42. Schröfelbauer, B., Chen, D., and Landau, N. R. (2004) A single amino acid of APOBEC3G controls its species-specific interaction with virion infectivity factor (Vif). *Proc. Natl. Acad. Sci. U.S.A.* **101,** 3927–3932
43. Bogerd, H. P., Doehle, B. P., Wiegand, H. L., and Cullen, B. R. (2004) A single amino acid difference in the host APOBEC3G protein controls the primate species specificity of HIV type 1 virion infectivity factor. *Proc. Natl. Acad. Sci. U.S.A.* **101,** 3770–3774
44. Mangeat, B., Turelli, P., Liao, S., and Trono, D. (2004) A single amino acid determinant governs the species-specific sensitivity of APOBEC3G to Vif action. *J. Biol. Chem.* **279,** 14481–14483
45. Miller, J. H., Presnyak, V., and Smith, H. C. (2007) The dimerization domain of HIV-1 viral infectivity factor Vif is required to block virion incorporation of APOBEC3G. *Retrovirology* **4,** 81
46. Kao, S., Khan, M. A., Miyagi, E., Plishka, R., Buckler-White, A., and Strebel, K. (2003) The human immunodeficiency virus type 1 Vif protein reduces intracellular expression and inhibits packaging of APOBEC3G (CEM15), a cellular inhibitor of virus infectivity. *J. Virol.* **77,** 11398–11407
47. Kao, S., Miyagi, E., Khan, M. A., Takeuchi, H., Opi, S., Goila-Gaur, R., and Strebel, K. (2004) Production of infectious human immunodeficiency virus type 1 does not require depletion of APOBEC3G from virus-producing cells. *Retrovirology* **1,** 27
48. Goila-Gaur, R., Khan, M. A., Miyagi, E., and Strebel, K. (2009) Differential sensitivity of "old" versus "new" APOBEC3G to human immunodeficiency virus type 1 vif. *J. Virol.* **83,** 1156–1160
49. Goila-Gaur, R., Khan, M. A., Miyagi, E., Kao, S., Opi, S., Takeuchi, H., and Strebel, K. (2008) HIV-1 Vif promotes the formation of high molecular mass APOBEC3G complexes. *Virology* **372,** 136–146
50. Camaur, D., and Trono, D. (1996) Characterization of human immunodeficiency virus type 1 Vif particle incorporation. *J. Virol.* **70,** 6106–6111
51. Kao, S., Akari, H., Khan, M. A., Dettenhofer, M., Yu, X. F., and Strebel, K. (2003) Human immunodeficiency virus type 1 Vif is efficiently packaged into virions during productive but not chronic infection. *J. Virol.* **77,** 1131–1140
52. Fouchier, R. A., Simon, J. H., Jaffe, A. B., and Malim, M. H. (1996) Human immunodeficiency virus type 1 Vif does not influence expression or virion incorporation of gag-, pol-, and env-encoded proteins. *J. Virol.* **70,** 8263–8269
53. Karczewski, M. K., and Strebel, K. (1996) Cytoskeleton association and virion incorporation of the human immunodeficiency virus type 1 Vif protein. *J. Virol.* **70,** 494–507
54. Mercenne, G., Bernacchi, S., Richer, D., Bec, G., Henriet, S., Paillart, J. C., and Marquet, R. (2010) HIV-1 Vif binds to APOBEC3G mRNA and inhibits its translation. *Nucleic Acids Res.* **38,** 633–646
55. Sadler, H. A., Stenglein, M. D., Harris, R. S., and Mansky, L. M. (2010) APOBEC3G contributes to HIV-1 variation through sublethal mutagenesis. *J. Virol.* **84,** 7396–7404
56. Nowarski, R., Britan-Rosich, E., Shiloach, T., and Kotler, M. (2008) Hypermutation by intersegmental transfer of APOBEC3G cytidine deaminase. *Nat. Struct. Mol. Biol.* **15,** 1059–1066
57. Xu, H., Chertova, E., Chen, J., Ott, D. E., Roser, J. D., Hu, W. S., and Pathak, V. K. (2007) Stoichiometry of the antiviral protein APOBEC3G in HIV-1 virions. *Virology* **360,** 247–256
58. Britan-Rosich, E., Nowarski, R., and Kotler, M. (2011) Multifaceted counter-APOBEC3G mechanisms employed by HIV-1 Vif. *J. Mol. Biol.* **410,** 1065–1076
59. Santa-Marta, M., da Silva, F. A., Fonseca, A. M., and Goncalves, J. (2005)

HIV-1 Vif can directly inhibit apolipoprotein B mRNA-editing enzyme catalytic polypeptide-like 3G-mediated cytidine deamination by using a single amino acid interaction and without protein degradation. *J. Biol. Chem.* **280,** 8765–8775
60. Greene, W. C., Debyser, Z., Ikeda, Y., Freed, E. O., Stephens, E., Yonemoto, W., Buckheit, R. W., Esté, J. A., and Cihlar, T. (2008) Novel targets for HIV therapy. *Antiviral Res.* **80,** 251–265
61. Zuo, T., Liu, D., Lv, W., Wang, X., Wang, J., Lv, M., Huang, W., Wu, J., Zhang, H., Jin, H., Zhang, L., Kong, W., and Yu, X. (2012) Small-molecule inhibition of human immunodeficiency virus type 1 replication by targeting the interaction between Vif and ElonginC. *J. Virol.* **86,** 5497–5507
62. Simon, V., Zennou, V., Murray, D., Huang, Y., Ho, D. D., and Bieniasz, P. D. (2005) Natural variation in Vif: differential impact on APOBEC3G/3F and a potential role in HIV-1 diversification. *PLoS Pathog.* **1,** e6
63. Jern, P., Russell, R. A., Pathak, V. K., and Coffin, J. M. (2009) Likely role of APOBEC3G-mediated G-to-A mutations in HIV-1 evolution and drug resistance. *PLoS Pathog.* **5,** e1000367
64. Pillai, S. K., Wong, J. K., and Barbour, J. D. (2008) Turning up the volume on mutational pressure: is more of a good thing always better? (a case study of HIV-1 Vif and APOBEC3). *Retrovirology* **5,** 26
65. Nguyen, K. L., llano, M., Akari, H., Miyagi, E., Poeschla, E. M., Strebel, K., and Bour, S. (2004) Codon optimization of the HIV-1 vpu and vif genes stabilizes their mRNA and allows for highly efficient Rev-independent expression. *Virology* **319,** 163–175
66. Le Grice, S. F., and Grüninger-Leitch, F. (1990) Rapid purification of homodimer and heterodimer HIV-1 reverse transcriptase by metal chelate affinity chromatography. *Eur. J. Biochem.* **187,** 307–314
67. Gao, F., Robertson, D. L., Morrison, S. G., Hui, H., Craig, S., Decker, J., Fultz, P. N., Girard, M., Shaw, G. M., Hahn, B. H., and Sharp, P. M. (1996) The heterosexual human immunodeficiency virus type 1 epidemic in Thailand is caused by an intersubtype (A/E) recombinant of African origin. *J. Virol.* **70,** 7013–7029
68. Briggs, J. A., Simon, M. N., Gross, I., Kräusslich, H. G., Fuller, S. D., Vogt, V. M., and Johnson, M. C. (2004) The stoichiometry of Gag protein in HIV-1. *Nat. Struct. Mol. Biol.* **11,** 672–675
69. Zhu, P., Chertova, E., Bess, J., Jr., Lifson, J. D., Arthur, L. O., Liu, J., Taylor, K. A., and Roux, K. H. (2003) Electron tomography analysis of envelope glycoprotein trimers on HIV and simian immunodeficiency virus virions. *Proc. Natl. Acad. Sci. U.S.A.* **100,** 15812–15817
70. Creighton, S., Bloom, L. B., and Goodman, M. F. (1995) Gel fidelity assay measuring nucleotide misinsertion, exonucleolytic proofreading, and lesion bypass efficiencies. *Methods Enzymol.* **262,** 232–256
71. Loeb, D. D., Swanstrom, R., Everitt, L., Manchester, M., Stamper, S. E., and Hutchison, C. A., 3rd. (1989) Complete mutagenesis of the HIV-1 protease. *Nature* **340,** 397–400
72. Chelico, L., Sacho, E. J., Erie, D. A., and Goodman, M. F. (2008) A model for oligomeric regulation of APOBEC3G cytosine deaminase-dependent restriction of HIV. *J. Biol. Chem.* **283,** 13780–13791
73. Huthoff, H., and Malim, M. H. (2007) Identification of amino acid residues in APOBEC3G required for regulation by human immunodeficiency virus type 1 Vif and virion encapsidation. *J. Virol.* **81,** 3807–3815
74. Lavens, D., Peelman, F., Van der Heyden, J., Uyttendaele, I., Catteeuw, D., Verhee, A., Van Schoubroeck, B., Kurth, J., Hallenberger, S., Clayton, R., and Tavernier, J. (2010) Definition of the interacting interfaces of Apobec3G and HIV-1 Vif using MAPPIT mutagenesis analysis. *Nucleic Acids Res.* **38,** 1902–1912
75. Cadima-Couto, I., Saraiva, N., Santos, A. C., and Goncalves, J. (2011) HIV-1 Vif interaction with APOBEC3 deaminases and its characterization by a new sensitive assay. *J. Neuroimmune Pharmacol.* **6,** 296–307
76. Bernacchi, S., Henriet, S., Dumas, P., Paillart, J. C., and Marquet, R. (2007) RNA and DNA binding properties of HIV-1 Vif protein: a fluorescence study. *J. Biol. Chem.* **282,** 26361–26368
77. Henriet, S., Richer, D., Bernacchi, S., Decroly, E., Vigne, R., Ehresmann, B., Ehresmann, C., Paillart, J. C., and Marquet, R. (2005) Cooperative and specific binding of Vif to the 5′ region of HIV-1 genomic RNA. *J. Mol. Biol.* **354,** 55–72
78. Henriet, S., Mercenne, G., Bernacchi, S., Paillart, J. C., and Marquet, R. (2009) Tumultuous relationship between the human immunodeficiency virus type 1 viral infectivity factor (Vif) and the human APOBEC-3G and APOBEC-3F restriction factors. *Microbiol. Mol. Biol. Rev.* **73,** 211–232
79. Uyttendaele, I., Lavens, D., Catteeuw, D., Lemmens, I., Bovijn, C., Tavernier, J., and Peelman, F. (2012) Random mutagenesis MAPPIT analysis identifies binding sites for Vif and Gag in both cytidine deaminase domains of Apobec3G. *PLoS One* **7,** e44143
80. Albin, J. S., LaRue, R. S., Weaver, J. A., Brown, W. L., Shindo, K., Harjes, E., Matsuo, H., and Harris, R. S. (2010) A single amino acid in human APOBEC3F alters susceptibility to HIV-1 Vif. *J. Biol. Chem.* **285,** 40785–40792
81. Smith, J. L., and Pathak, V. K. (2010) Identification of specific determinants of human APOBEC3F, APOBEC3C, and APOBEC3DE and African green monkey APOBEC3F that interact with HIV-1 Vif. *J. Virol.* **84,** 12599–12608
82. Kitamura, S., Ode, H., Nakashima, M., Imahashi, M., Naganawa, Y., Kurosawa, T., Yokomaku, Y., Yamane, T., Watanabe, N., Suzuki, A., Sugiura, W., and Iwatani, Y. (2012) The APOBEC3C crystal structure and the interface for HIV-1 Vif binding. *Nat. Struct. Mol. Biol.* **19,** 1005–1010
83. Nathans, R., Cao, H., Sharova, N., Ali, A., Sharkey, M., Stranska, R., Stevenson, M., and Rana, T. M. (2008) Small-molecule inhibition of HIV-1 Vif. *Nat. Biotechnol.* **26,** 1187–1192
84. Browne, E. P., Allers, C., and Landau, N. R. (2009) Restriction of HIV-1 by APOBEC3G is cytidine deaminase-dependent. *Virology* **387,** 313–321